Preprint 20230926v1.0 doi:10.5281/zenodo.8415031

Quantifying the visual impact of wind farm lights on the nocturnal landscape

Salvador Bará [1] and Raul C. Lima [2,3]

[1] *Former profesor titular (retired) at Universidade de Santiago de Compostela (USC), Santiago de Compostela, 15782 Galicia (Spain, European Union)*

[2] *Física, Escola Superior de Saúde, Politécnico do Porto, Portugal*

[3] *IA – Instituto de Astrofísica e Ciências do Espaço, Univ Coimbra, Portugal*

e-mail: salva.bara@usc.gal, raulcpslima@ess.ipp.pt

Abstract: Wind farm lights are a conspicuous feature in the nocturnal landscape. Their presence is a source of light pollution for residents and the environment, severely disrupting in some places the aesthetic, cultural, and scientific values of the pristine starry skies. In this work we present a simple model for quantifying the visual impact of individual wind turbine lights, based on the comparison of their brightnesses with the brightness of well-known night sky objects. The model includes atmospheric and visual variables, and for typical parameters it shows that medium-intensity turbine lights can be brighter than Venus up to ∼4 km from the turbine, brighter than α CMa (the brightest star on the nighttime sky) until about ∼10 km, and reach the standard stellar visibility limit for the unaided eye ($m_v = +6.00$) at ∼38 km. These results suggest that the visual range of wind farms at nighttime may be significantly larger than at daytime, a factor that should be taken into account in environmental impact assessments.

1. Introduction

The need to reduce dependence on fossil fuels has fostered the development of renewable energy sources. This process has been accelerated in the last years due to the pressing urgence to address anthropogenic climate change and achieve higher levels of energy sovereignty. Among renewable sources, wind power energy is nowadays a crucial player.

The installation of new wind power facilities, both onshore and offshore, has not come without problems. Wind farms generate a wide range of environmental impacts (Leung and Yang, 2012; Saidur et al, 2011), including but not limited to serious avian (Hüppop et al, 2006; Kerlinger et al, 2010; Marques et al, 2014) and bat fatalities due to collisions (Kunz et al, 2007; Rodrigues et al, 2022; Voigt et al, 2022; Smallwood, 2013). The sustainability of large offshore

wind farms, planned or in construction, has been subjected to critical review in some recent European evaluations (ECA, 2023; Lloret et al, 2023).

Besides their effects on biodiversity, wind farms also affect humans through the combined impacts of noise, lights (direct obstruction lights and stroboscopic effects of rotating blade shadows), and visual landscape degradation (Lothian, 2008). The annoyance produced by wind farm lights on neighboring communities has deserved growing attention in recent times (Bjørn et al, 2022; Pohl et al, 2012, 2021; Rudolph et al, 2017).

The visual landscape degradation produced by wind farms has been evaluated mostly for daytime, based on turbine visibility estimates (limited by the contrast luminance thresholds in daylight) combined with different spatial aggregation metrics (see e.g. Hurtado et al, 2004; Kokologos et al, 2014). Comparatively less attention has been given to the deleterious effects of wind farm lights on the nighttime landscape (Fig. 1). The nightscape is an essential element of the human experience, whose cultural, social, scientific, and aesthetic values are assets of the intangible heritage of humankind (Marín and Jafari, 2008). As set forth by the Natural Sounds and Night Skies Division of the USA National Parks Service "a naturally dark night sky is more than a scenic canvas; it is part of a complex ecosystem that supports both natural and cultural resources" (NPS, 2021). Borrowing from Rich and Longcore (2006) on conservation planning, it can certainly be said that daytime landscapes are "only half the story–the daytime story".

Fig. 1. Nigthtime landscape with wind farm obstruction lights in Miranda do Corvo, Serra da Lousã, Portugal (40°02'42.98”N, 8°16'30.84” W). Image credit: Raul C. Lima.

In this work we present a model for quantifying the primary visual effect of wind farm lights on the nocturnal landscape. It is based on considering wind farm lights as artificial stars and applying to them the metrics used in visual astronomy to quantify their perceived brightness. That way they can be compared with the stars and other natural bodies present on the sky, facilitating an easy and intuitive evaluation of the disruption caused to the pristine nightscape. The model incorporates atmospheric and perceptual parameters. Although it is formulated in terms of human-based photometric (in lighting engineering language) or visual band (in astronomical language) quantities, its generalization for arbitrary spectral distributions and

observation bands is immediate. This visibility model provides the basic building block from which overall visual impact assessments can be derived with the help of different spatial aggregation metrics.

2. Methods

2.1. Retinal images of resolved and unresolved objects

The visual brighness of an object depends on several radiometric and anatomical factors, besides the physiological and neural ones. The basic inputs to the visual system are the photon catches of the retinal photoreceptor cells. The number of photons captured by an individual photoreceptor in each wavelength interval $[\lambda, \lambda + \Delta\lambda]$ during the time Δt is proportional to $S(\lambda)\ E'(\lambda)\ \Delta\lambda\ \Delta t$, where $S(\lambda)$ is the spectral sensitivity of the photoreceptor and $E'(\lambda)$ is the spectral irradiance of the object's retinal image at the photoreceptor location. Wavelength values are here referred to vacuum.

The spectral irradiance is defined as the radiant flux (photons·s^{-1}) per unit surface and unit wavelength interval, and is measured in photons·s^{-1}·m^{-2}·nm^{-1}. The spectral irradiance $E'(\lambda)$ at each retinal location can be approximately described by:

$$E'(\lambda) = T_e(\lambda)\ L(\lambda)\ \omega \frac{A_p}{A_i} \cos\theta \tag{1}$$

where $T_e(\lambda)$ is the spectral transmittance of the ocular media (unitless), $L(\lambda)$ is the object radiance (photons·s^{-1}·m^{-2}·sr^{-1}·nm^{-1}), ω is the solid angle (sr) subtended by the object as seen from the observer, A_p is the area of the input pupil of the eye (m^2), A_i is the area of the retinal image (m^2), and θ is the angle between the direction in which the object lies and the line perpendicular to the eye pupil. Eq.(1) can be equivalently rewritten in terms of $E(\lambda) = L(\lambda)\ \omega \cos\theta$, the spectral irradiance produced by the object on the eye pupil, as:

$$E'(\lambda) = T_e(\lambda)\ E(\lambda)\ \frac{A_p}{A_i} \tag{2}$$

In a perfect imaging system, according to geometrical optics, the image would be an exact scaled replica of the object. The area of the image would be proportional to the solid angle subtended by the object, ω, such that $A_i = \kappa\ \omega$, being κ a constant (units m^2) independent from the object. For a perfect imaging system, then, the object feature that determines the input to the photoreceptor cells is its spectral radiance, $L(\lambda)$, since the solid angle ω cancels out in Eq.(1):

$$E'(\lambda) = T_e(\lambda)\ L(\lambda)\ \frac{A_p}{\kappa} \cos\theta \tag{3}$$

and the remaining factors only depend on the eye.

Human eyes, however, are not perfect optical instruments. The eye optics deforms the ideal images to a bigger or lesser extent due to diffraction by the finite size of the eye pupil (Born and Wolf, 1999), refractive errors including both classical ametropies and high-order optical defects (Liang et al, 1994; Losada and Navarro, 1998; Navarro and Losada, 1997a; Navarro et al, 1998), and intraocular scattering due to small-scale inhomogeneities of the eye media (van den Berg et al, 2010, 2013; Bará and Bao-Varela, 2022). The retinal image in a real eye is no longer an exact scaled replica of the object itself.

The actual image of an object on the human retina is given by the two-dimensional convolution of the ideal geometric image with the point-spread function of the eye, PSF (Goodman, 1996). The PSF is the function that describes how the eye optics deforms the image of an ideal point source. Human eyes present a high variability of PSF sizes and shapes (Castejón-Mochón et al, 2002; Guirao et al, 2002; Liang and Williams, 1997; Porter et al, 2001; Thibos et al, 2002a, 2002b). This convolution gives rise to a new irradiance distribution that combines the features of the convolved functions. The retinal image can be interpreted as 'blurred' version of the perfect geometrical image, in which each point has been replaced by a PSF proportional to the object radiance at that point and the resulting irradiances have been added up.

In the limiting case of *well resolved objects*, that is, when the angular size of the object is much larger than the angular size of the PSF, the result of the convolution is a slightly blurred version of the ideal geometrical image, and Eq.(3) still approximately applies.

Conversely, when the angular size of the object viewed by the observer is substantially smaller than the angular size of the eye's PSF, as it happens e.g. with a star or distant streetlight, the retinal image is essentially equal to the PSF itself. In such cases, one may speak of *unresolved objects.* The retinal images of unresolved objects located in different directions of the central visual field are just replicas of the PSF centered in different retinal points. All these images have the same shape and size, only differing in brightness (Bará, 2013; Navarro and Losada, 1997b; Navarro et al., 1998).

This result has important visual consequences. One of them is that the main physical factor that determines the perceived brightness of an unresolved object is not the intrinsic object's radiance, as in the well-resolved case, but the irradiance $E(\lambda)$ it produces on the eye pupil. This happens because the area of the retinal image is no longer proportional to the object's solid angle, as in case of a perfect system ($A_i = \kappa\,\omega$), but it is constant and equal to the area of the PSF, $A_i = A_{PSF}$. For an unresolved object Eq.(2) becomes:

$$E'(\lambda) = T_e(\lambda)\,E(\lambda)\,\frac{A_p}{A_{PSF}} \tag{4}$$

in which the object intervenes through $E(\lambda)$, since the remaining factors depend only on the eye.

In terms of human visual (photometric) quantities, irradiances and radiances outside the eye correspond to illuminances and luminances, respectively. The illuminance E_{v}, measured in

lux (lx), is the integral over wavelengths of the spectral irradiance $E(\lambda)$ weighted by the photopic luminous efficiency function $V(\lambda)$ and multiplied by the luminous efficacy constant 683 lm/W (CIE, 1990). The luminance L_{v}, measured in candela per square meter (cd·m^{-2}), is the analogous integral applied to the spectral radiance $L(\lambda)$. The cd is the unit of luminous intensity, I_{v}, (1 cd=1 lm·sr^{-1}) being the only basic unit of the International System (BIPM, 2019) whose definition is strictly tied to human visual perception. The cd links perceptual to physical stimuli, and by its own definition it takes implicitly into account the transmittance of the ocular media, $T_e(\lambda)$, the spectral sensitivity of the photoreceptors, $S(\lambda)$, and the basic neural processes related to the perception of luminance.

2.2. Illuminance produced by wind turbine lights on the eye pupil of the observer

The illuminance E_{v} produced by an unresolved wind turbine light on the eye pupil of an observer located a distance r away is:

$$E_{\mathrm{v}}(r,\theta) = T(r)\, I_{\mathrm{v}}(\theta)\, \frac{\cos\theta}{r^2} \tag{5}$$

where $T(r)$ is the atmospheric transmittance accounting for the reduction of the beam intensity due to absorption and scattering by the molecular and aerosol constituents of the atmosphere, $I_{\mathrm{v}}(\theta)$ is the luminous intensity of the wind turbine light sent towards the observer and θ is the angle between the normal to the pupil and the direction where the wind turbine light is located. This equation, published in simplified form by Allard one and a half century ago (Allard, 1876; Bullough, 2011) stems from the basic definition of these photometric quantities and the properties of light propagation in attenuating media. The formulation of Eq.(5) in terms of the luminous intensity of the wind turbine lights I_{v} is particularly useful, because this is the photometric quantity specified for the different types of obstruction lights in the ICAO recommendations (ICAO, 2018), and whose values have been generally adopted by the wind farm legislations, e.g. AESA (2017).

For a layered atmosphere, light propagation paths at angles close to the horizontal, and direct visual fixation on the turbine light ($\theta = 0°, \cos\theta = 1$), Eq.(5) becomes

$$E_{\mathrm{v}}(r) = I_{\mathrm{v}}\, \frac{e^{-kr}}{r^2} \tag{6}$$

where $I_{\mathrm{v}} = I_{\mathrm{v}}(0°)$, and the atmospheric transmittance $T(r)$ is described by the Bouger-Lambert exponential law $T(r) = e^{-kr}$, being k the combined molecular and aerosol attenuation coefficient per unit length (m^{-1}) at the average altitude above sea level of observer and lights.

2.3. How bright are wind turbine lights compared to the stars and planets of the natural sky?

The visual brightness of the stars and other unresolved point-like sources on the sky is commonly reported in astronomy in terms of "astronomical magnitudes". The astronomical magnitude is a negative logarithmic scale for expressing the in-band irradiance produced by a

star, relative to some reference irradiance. This scale was qualitatively introduced by Hipparchus (c. 190–c. 120 BC) and formalized in the 19th century (Pogson, 1856). The magnitude scale is also applied to illuminances E_{v}, taking as traditional reference the illuminance of the star Vega (α Lyr) at the top of the terrestrial atmosphere, $E_{\mathrm{v,ref}} = E_{\mathrm{v,Vega}} = 2.54 \times 10^{-6}$ lx (Allen, 1973; Bará, 2017; Bará et al., 2020). According to the basic definition of this scale, an unresolved celestial object producing an illuminance E_{v} (in lx) at the top of the terrestrial atmosphere has a magnitude m_{v} given by

$$m_{\mathrm{v}} = -2.5 \log_{10}\left(\frac{E_{\mathrm{v}}}{E_{\mathrm{v,ref}}}\right) \tag{7}$$

Conversely, the illuminance at the top of the atmosphere in terms of the magnitude is

$$E_{\mathrm{v}} = E_{\mathrm{v,ref}} \times 10^{-0.4\, m_{\mathrm{v}}} \quad \text{(lx)} \tag{8}$$

It is conventionally but somehow arbitrarily accepted that an average observer may detect stars up to $m_{\mathrm{v}} \approx 6.0$. As a matter of fact, the limiting visual magnitude of the unaided eye depends on many factors, including the luminance contrast threshold of the observers at the luminance adaptation level they are experiencing, the state of the atmosphere, and the artificial skyglow and glare (two effects of light pollution) at the observer location. For a detailed analysis see Schaefer (1993), Cinzano and Falchi (2020), and Bará and Bao-Varela (2022).

When a star is observed from the ground, its extra-atmospheric illuminance is reduced due to the attenuation undergone by the light rays along their path through the atmosphere. This can be accounted for by an atmospheric transmittance term

$$T_{atm}(z) = \exp\{-M(z)\, \tau\} \tag{9}$$

where z is the angle from the star to the zenith, τ is the atmospheric vertical optical depth, and $M(z)$ is the air mass number. The atmospheric optical depth is given by $\tau = \tau_m + \tau_a$, where τ_m and τ_a are the molecular (MOD) and aerosol (AOD) optical depths, respectively, defined in terms of the corresponding vertical profiles of the molecular $k_m(h)$, and aerosol, $k_a(h)$, extinction coefficients (Kocifaj, 2007) as:

$$\tau_i = \int_{h=0}^{\infty} k_i(h)\, \mathrm{d}h \qquad i \in \{m, a\} \tag{10}$$

For an exponential atmosphere in which k_m and k_a decrease exponentially with the altitude h, with scale heights H_m and H_a, respectively, we have

$$\tau_i = \int_{h=0}^{\infty} k_i(0)\, e^{-h/H_i}\, \mathrm{d}h = k_i(0)\, H_i \qquad i \in \{m, a\} \tag{11}$$

being $k_i(0)$ the value of the attenuation coefficients at ground level. Typical values for the exponential scale heights are $H_m = 8$ km and H_a=1.5 km. The value of τ_m at sea level at the center of the visible spectrum is about 0.09-0.11, see Teillet (1990) for detailed expressions, and the aerosol optical depth τ_a may range typically from 0.1 or smaller for clear atmospheres

to 0.5 and larger for more turbid ones, being able to reach much higher values (Dubovik et al., 2002; Hess et al., 1998; Giles et al., 2019). Note that the coefficient k appearing in Eq.(6) can be written as

$$k = k_m(0) + k_a(0) = \frac{\tau_m}{H_m} + \frac{\tau_a}{H_a} \tag{12}$$

Regarding the airmass factor, for zenith angles not extremely close to the horizon its value can be calculated as $M(z) = 1/\cos z$. The number of air masses increases very quickly at angles close to the horizon, for which more accurate expressions shall be used (Kasten and Young, 1989). For the zenith, $M(0°) = 1$.

The atmospheric transmittance in Eq.(9) can be expressed as an equivalent extinction value $m_{ext}(z)$ in magnitudes. The magnitude $m_{\mathrm{v}}(z)$ of a star observed from ground at a zenith angle z (angle above the horizon $90° - z$) is:

$$m_{\mathrm{v}}(z) = -2.5 \log_{10}\left[\frac{T_{atm}(z)\, E_{\mathrm{v}}}{E_{\mathrm{v,ref}}}\right] = -2.5 \log_{10}\left(\frac{E_{\mathrm{v}}}{E_{\mathrm{v,ref}}}\right) - 2.5 \log_{10}[T_{atm}(z)] \tag{13}$$

that can be rewritten as

$$m_{\mathrm{v}}(z) = m_{\mathrm{v}} + m_{ext}(z) \tag{14}$$

being m_{v} the extra-atmospheric magnitude given by Eq.(7), and $m_{ext}(z)$ the extinction term $m_{ext}(z) = 2.5\, M(z)\, \tau \log_{10}(e)$. Recall that larger (= more positive) values of $m_{\mathrm{v}}(z)$ correspond to dimmer objects, due to the negative sign of the log scale magnitude definition.

The brightness of the wind farm lights can also be expressed in astronomical magnitudes, allowing that way comparing them with the natural stars. This could be done in a naïve way by directly applying Eq.(7) to the illuminance produced by the lights on the observer's eye pupil, $E_{\mathrm{v}}(r)$, given in Eq.(6). There is, however, an issue that shall be kept in mind. Whereas the astronomical magnitudes refer to the irradiance produced by a celestial object *at the top* of the atmosphere, the light from wind farms reaches the observer after propagating some finite distance nearly horizontally *at the bottom* of the atmosphere. Furthermore, the brightness of a star seen from ground is not constant, but depends on its altitude above the horizon, or, equivalently, on its corresponding zenit angle z as set forth in Eq.(13). Comparing the visual appearance of wind farm lights with the appearance of stars requires choosing first a reference altitude above the horizon at which the comparison stars are seen.

Once the reference zenith distance z is chosen, one can easily assign to the wind farm light the extra-atmospheric magnitude m_{v} of a star whose brightness at this z would be the same as the brightness of the wind farm light perceived by the observer. According to Eqs.(6)-(7) this magnitude is:

$$m_{\mathrm{v}} = -2.5 \log_{10}\left[\frac{I_{\mathrm{v}}\, e^{-kr}}{r^2\, T_{atm}(z)\, E_{\mathrm{v,ref}}}\right] \tag{15}$$

Note that the transmittance $T_{atm}(z)$ is in the denominator, since we are calculating the extra-atmospheric irradiance that would result in the irradiance $E_{\mathrm{v}}(r)$ at ground level after

propagating through the atmosphere at a zenith angle z. This can alternatively be interpreted as using a reduced $T_{atm}(z)\ E_{\mathrm{v,ref}}$ reference illuminance for establishing the 'zero point' of a new magnitude scale defined on irradiances at ground level, not at the top of the atmosphere.

Regarding the choice of z, comparing the wind farm lights with stars at the zenith (altitude 90°, z=0°, $M(0°) = 1$) is always an option, although to perform in practice this comparison the observers should successively direct their gaze horizontally to the wind farm and vertically to the zenith sky, because the possibility of simultaneous viewing (although theoretically possible, given the size of the monocular field of view of the human eye along the vertical axis, ~60° upward and ~75° downward) would require that both light sources were imaged in diametrally opposed locations of the peripheral retina. Comparing wind farm lights with stars at the horizon would neither be a practical choice, since the attenuation of starlight in that direction is usually extremely high excepting for very clear atmospheres ($\tau \ll 0.05$), due to the large number of air masses, $M(90°) \approx 38$ (Kasten and Young, 1989). For instance, for $\tau = 0.2$ the extinction at the horizon is of order $m_{ext}(90°) = +8.25$ magnitudes. For our present purposes an intermediate altitude above the horizon, well within the visual field of an observer looking horizontally at the lights, is appropriate. For the following sections we will use a reference altitude of 30° ($z = 60°$, $M(60°) = 2.0$). The conversion of our results for other possible choices of the altitude above the horizon of the comparison stars is immediate.

3. Results

Figure (2) shows the equivalent top-of-the-atmosphere (TOA) astronomical magnitude m_{v} of a wind farm light (for a reference altitude of 30° degrees above horizon, $z = 60°$, $M(60°) = 2.0$), as a function of the distance to the viewer, r. The atmospheric parameters are $\tau_m = 0.10$, $\tau_a = 0.20$, $H_m = 8000$ m and H_a=1500 m. The results were calculated for nighttime obstruction lights of medium-intensity, $I_{\mathrm{v}} = 2000$ cd, and for two levels of low-intensity, $I_{\mathrm{v}} = 200$, and I_{v} =40 cd (AESA, 2017; ICAO, 2018). The extinction coefficient at ground level is $k = 1.46 \times 10^{-4}$ m^{-1}, corresponding to a daytime visual range of ~26 km. The horizontal lines show the astronomical magnitudes in the Johnson-Cousins V band (Bessell, 1990) of several conspicuous objects on the sky, namely the Moon, $m_{\mathrm{v}} = -12.73$ (full Moon at mean distance from Earth, near opposition but not including the opposition surge, Allen, 1973, p. 144), Venus, $m_{\mathrm{v}} = -4.22$ (mean magnitude of Venus, at maximum elongation, Allen *op. cit.* p. 144), and the star Sirius (α CMa), $m_{\mathrm{v}} = -1.45$ (Allen *op. cit.* p. 240). The standard human star visibility limit with the unaided eye, $m_{\mathrm{v}} = +6.00$, is also shown. In the Johnson-Cousins V band the magnitude of the star Vega (α Lyr) is usually set at $m_{\mathrm{v}} = +0.03$. Fig 2(a) shows the magnitude values within the 0.01-50 km distance range, whereas Fig 2(b) shows an enlarged view of the first 5 km from the lights.

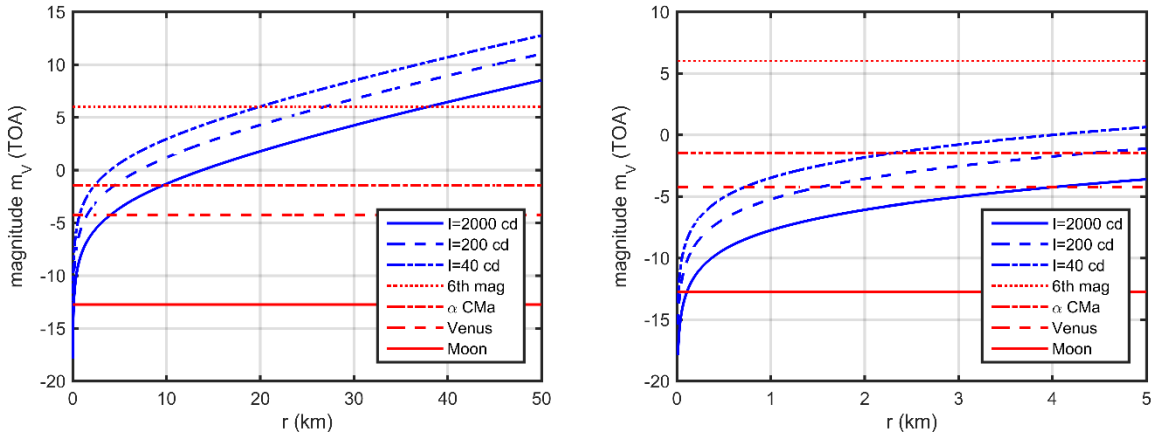

Fig. 2. Equivalent top-of-the-atmosphere (TOA) astronomical magnitude m_v of wind turbine lights seen from distances r, Eq.(15), for lamps of luminous intensities $I_v = 2000$, 200, and 40 cd, and an atmosphere with AOD $\tau_a = 0.2$ and (see text for details). (a) range 0.01- 50 km, (b) enlarged view of the range 0.01-5.0 km.

It can be seen in Fig.(2) that the nighttime lights of $I_v = 2000$ cd widely used in wind turbines of height between 100 and 150 m (AESA, 2017) can be brighter than Venus up to 4 km from the turbine, brighter than α CMa up to about 10 km, and reach the visibility limit $m_v = +6.00$ at 38 km. These results suggest that the visual range of wind farms at nighttime in pristine sites (limited by the luminous intensity of the lamps and the atmospheric attenuation) may be significantly higher than at daytime (limited by the luminance contrast thresholds applied to sunlight scattered into the line of sight (Bohren and Clothiaux, 2006)).

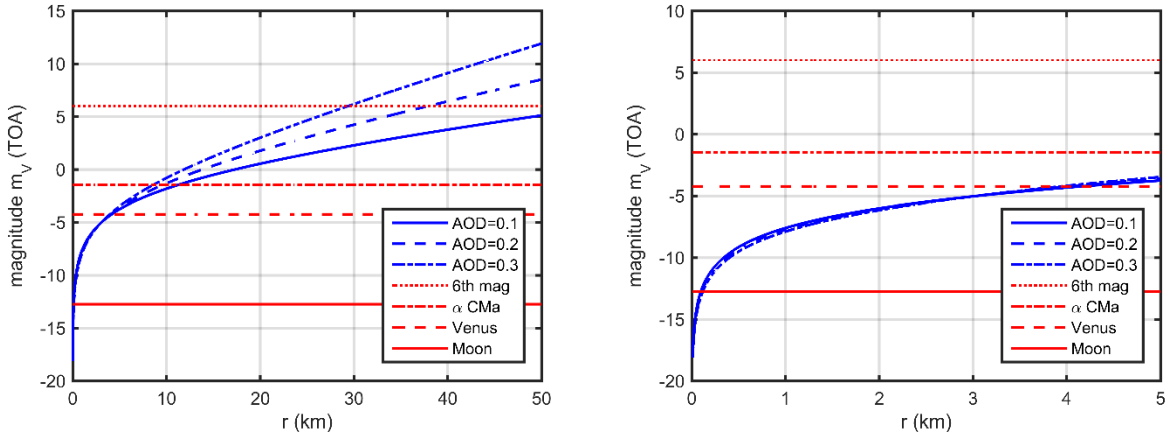

Fig. 3. Equivalent top-of-the-atmosphere (TOA) astronomical magnitude m_v of wind turbine lights seen from distances r, Eq.(15), for lamps of luminous intensity I_v=2000 cd and atmospheres with AODs τ_a= 0.1, 0.2 and 0.3 (see text for details). (a) range 0.01- 50 km, (b) enlarged view of the range 0.01-5.0 km.

Figure (3) shows the magnitudes m_{v} for lights of constant luminous intensity ($I_{\mathrm{v}} = 2000$ cd) and three different aerosol optical depths, $\tau_a = 0.1$, 0.2 and 0.3, corresponding to daytime visual ranges of 49 km, 26 km, and 18 km, respectively, the remaining parameters being the same as in Fig.(1). During the first kilometers from the lamps the change in visual magnitude is dominated by the geometrical factor $1/r^2$ in Eq. (15), with little influence of the horizontal-path atmospheric attenuation e^{-kr}, so the m_{v} curves for different AOD are very close to each other. As the distance increases, the horizontal atmospheric attenuation becomes dominant and the values of m_{v} increase almost linearly with r. The overall behavior is also function of the value of $T_{atm}(z = 60°)$, the atmospheric attenuation for an equivalent star seen at 30° above the horizon (here, two air masses), the reason behind the fact that the curves do not fully overlap in the first few km from the sources.

4. Discussion

The results obtained in Sect. 3 using the main equation of this work, Eq.(15), show that wind turbine lights can compete with natural sky objects up to distances in the range of tens of km. This has a non-negligible effect on the nocturnal landscape, particularly so because these lights are normally seen close to the horizon, towards which very often the human direction of gaze is oriented.

The calculations in Sect. 3 were made under some simplifying assumptions and can be generalized without difficulty to account for additional factors, as e.g. the relative and absolute altitudes above sea level of observers and lights (here assumed to be equal), the change of the luminous intensity of the wind farm lamps with the emission angle, or the spectral dependence of the conversions between Johnson-Cousin V magnitudes and luminances. Also, we have assumed photopically adapted observers (that is, observers who are looking at the lights from windows of lit spaces indoors or shortly after leaving illuminated areas outdoors). The calculations for mesopic or scotopic adaptation states can be easily done if some additional information about the wind farm light spectra is available (see, e.g Bará et al., 2020; Fryc et al., 2021).

In Sect. 3 it has been implicitly assumed that, although each wind turbine light is seen as an unresolved object, different lights are enough separated angularly among themselves as to ensure that the corresponding PSFs do not significantly overlap in the observer's retina. The objects can then then perceived independently, the attention may shift from one to another (Landau and Fries, 2012), the detection thresholds remain unaltered (Greve, 1972), and their magnitudes m_{v} are correctly described by Eq.(15) using the I_{v} of each individual lamp. However, on some occasions several distant lights may happen to be angularly very close, as seen from the observer, such that their PSFs substantially overlap in the retina. In that case they would appear as a single and brighter (but still unresolved) object, and its resulting magnitude m_{v} shoud be calculated by adding first the iluminances $E_{\mathrm{v}}(r)$ produced by each lamp on the eye pupil, Eq.(6), taking into account their possibly different distances and luminous intensities, and then applying Eq.(15) to the total $E_{\mathrm{v}}(r)$ resulting from this sum.

The basic model presented in this work allows for an easy quantification of the visual impact of individual wind farm lights on the nocturnal landscape, by direct comparison of their brightness with the brightness of well-known and conspicuous objects of the pristine starry sky. An issue that has not been addressed here and that deserves further consideration is the quantification of the aggregated impact of high numbers of wind farm lights shining simultaneously across large stretches of the horizon, a not uncommon situation in areas with very high density of turbines. Metrics developed for quantifying aggregated impacts during daytime (Hurtado et al, 2004; Kokologos et al, 2014) offer some interesting starting points. Besides its direct application to landscape assessment, it may be of potential interest for professional astronomy, whose ground-based observatories are subjected to an increasing stress by the presence and effects of artificial lights (Falchi et al, 2023; Green at al, 2022).

5. Conclusions

Wind farm lights are a source of light pollution in the nocturnal landscape. In this work we quantify the impact of individual light sources by comparing their perceived brightness with the brightness of the stars and other conspicuous bodies of the starry night sky. For typical parameters of the lights and the atmosphere our model shows that medium-intensity turbine lights can be brighter than Venus up to ∼4 km distance, brighter than α CMa (the brightest star on the nighttime sky) up to about ∼10 km, and reach the standard stellar visibility limit for the unaided eye ($m_v = +6.00$) at ∼38 km. These results suggest that the visual range of wind farms at nighttime may be considerably larger than at daytime. This factor should be taken into account in environmental impact assessments.

References

AESA – Agencia Estatal de Seguridad Aérea. 2017. *Guía de Señalamiento e Iluminación de Turbinas y Parques Eólicos*. https://www.seguridadaerea.gob.es/sites/default/files/ssaa-17-gui-126-a01.pdf (accessed 2 September 2023)

Allard É. 1876. *Mémoire sur l'intensité et la portée des phares*. Paris, France: Imprimerie Nationale. p. 74

Allen CW. 1973. *Astrophysical Quantities*, 3d ed. London: Athlone Press. p. 197

Bará S. 2013. The sky within your eyes (Eye aberrations and visual Astronomy), Sky and Telescope 126(2): 68-71.

Bará S. 2017. Variations on a classical theme: On the formal relationship between magnitudes per square arcsecond and luminance, International Journal of Sustainable Lighting 19(2): 104-111. https://doi.org/10.26607/ijsl.v19i2.77

Bará S. Aubé M, Barentine J, Zamorano J. 2020. Magnitude to luminance conversions and visual brightness of the night sky. Monthly Notices of the Royal Astronomical Society 493: 2429–2437. https://doi.org/10.1093/mnras/staa323

Bará S, Bao-Varela C. 2023. Skyglow inside your eyes: intraocular scattering and artificial brightness of the night sky. International Journal of Sustainable Lighting, 2023: 1-9. https://doi.org/10.26607/ijsl.v25i01.130

Bessell MS. 1990. UBVRI Passbands. Publications of the Astronomical Society of the Pacific 102: 1181–1199. https://doi.org/10.1086/132749

BIPM 2019. *Proceedings of the 26th meeting of the General Conference on Weights and Measures (2018)*. Sèvres, France: Bureau international des poids et mesures. p. 472. https://doi.org/10.59161/CGPM2018RES1E

Bjørn S, Lyhne I, Philipp D, Nedergaard H, Tolnov L, Kirch J. 2022. Do demand-based obstruction lights on wind turbines increase community annoyance? Evidence from a Danish case, Renewable Energy 192: 164-173. https://doi.org/10.1016/j.renene.2022.04.127

Bohren CF, Clothiaux EE. 2006. *Fundamentals of Atmospheric Radiation*. Berlin: Wiley-VCH. 415-416. https://doi.org/10.1002/9783527618620

Born M, Wolf, E. 1999. *Principles of Optics*, 7th ed. Cambridge, UK: Cambridge University Press, pp. 439-443.

Bullough JD. 2011. Aviation Signal Lighting: Impacts of Lighting Characteristics on Visibility. Adv. Appl. Sci. Res. 2: 16–27.

Castejón-Mochón JF, López-Gil M., Benito A, Artal P. 2002. Ocular wave-front aberration statistics in a normal young population. Vision Research 42: 1611-1617.

CIE – Commision Internationale de l'Éclairage. 1990. CIE 1988 2° Spectral Luminous Efficiency Function for Photopic Vision. CIE 86:1990. Vienna: Bureau Central de la CIE.

Cinzano P, Falchi F. 2020. Toward an atlas of the number of visible stars. Journal of Quantitative Spectroscopy & Radiative Transfer 253: 107059

Dubovik O, Holben B, Eck TF, Smirnov A, Kaufman YJ, King MD, et al. 2002. Variability of absorption and optical properties of key aerosol types observed in worldwide locations. J Atmos Sci 59: 590-608. https://doi.org/10.1175/1520-0469(2002)059<0590:VOAAOP>2.0.CO;2

ECA. 2023. *Special report 22/2023: Offshore renewable energy in the EU – Ambitious plans for growth but sustainability remains a challenge*. European Court of Auditors 18/09/2023. Luxembourg: Publications Office of the European Union. https://www.eca.europa.eu/en/publications/SR-2023-22

Falchi F, Ramos F, Bará S, Sanhueza P, Jaque-Arancibia M, Damke G, Cinzano P. 2023. Light pollution indicators for all the major astronomical observatories. Monthly Notices of the Royal Astronomical Society 519(1): 26–33, https://doi.org/10.1093/mnras/stac2929

Fryc I, Bará S, Aubé M, Barentine JC, Zamorano J. 2022. On the Relation between the Astronomical and Visual Photometric Systems in Specifying the Brightness of the Night Sky for Mesopically Adapted Observers. Leukos 18(4): 447-458. https://doi.org/10.1080/15502724.2021.1921593

Giles DM, Sinyuk A, Sorokin MG, Schafer JS, Smirnov A, Slutsker I, Eck TF, Holben BN, Lewis JR, Campbell JR, Welton EJ, Korkin SV, Lyapustin AI. 2019. Advancements in the Aerosol Robotic

Network (AERONET) Version 3 database – automated near-real-time quality control algorithm with improved cloud screening for Sun photometer aerosol optical depth (AOD) measurements. Atmos. Meas. Tech. 12:169–209. https://doi.org/10.5194/amt-12-169-2019, 2019.

Goodman JW. 1996. *Introduction to Fourier Optics*, 2nd. ed. New York: McGraw-Hill. pp. 134.

Green RF, Luginbuhl CB, Wainscoat RJ et al. 2022. The growing threat of light pollution to ground-based observatories. Astron Astrophys Rev 30: 1. https://doi.org/10.1007/s00159-021-00138-3

Greve EL. 1972. Single stimulus and multiple stimulus threshold Vision Research 12(9): 1533-1543. https://doi.org/10.1016/0042-6989(72)90178-2

Guirao A, Porter J, Williams DR, Cox IG. 2002. Calculated impact of higher-order monochromatic aberrations on retinal image quality in a population of human eyes. J. Opt. Soc. Am A 19: 620-628.

Hess M, Koepke P, Schult I. 1998. Optical Properties of Aerosols and Clouds: The Software Package OPAC, Bulletin of the American Meteorological Society, 79(5): 831-844.

Hüppop O, Dierschke J, Exo K-M, Fredrich E, Hill R. 2006. Bird migration studies and potential collision risk with offshore wind turbines. Ibis 148: 90–109. https://doi.org/10.1111/j.1474-919X.2006.00536.x

Hurtado JP, Fernandez J, Parrondo JL, Blanco E. 2004. Spanish method of visual impact evaluation in wind farms. Renew. Sustain. Energy Rev. 8(5): 483–491. https://doi.org/10.1016/j.rser.2003.12.009

ICAO. 2018. Annex 14, *Aerodromes*, Volume 1 Aerodrome Design and Operations, Eighth Edition, Montréal, Quebec, Canada: International Civil Aviation Organization. pp. 197-210.

Kasten F, Young AT. 1989. Revised optical air mass tables and approximation formula. Applied Optics 28(22): 4735-4738. https://doi.org/10.1364/AO.28.004735

Kerlinger P, Gehring JL, Erickson WP, Curry R, Jain A, Guarnaccia J. 2010. Night Migrant Fatalities and Obstruction Lighting at Wind Turbines in North America. The Wilson Journal of Ornithology 122(4): 744-754. https://doi.org/10.1676/06-075.1

Kocifaj M. (2007). Light-pollution model for cloudy and cloudless night skies with ground-based light sources, Appl. Opt. 46: 3013-3022. https://doi.org/10.1364/AO.46.003013

Kokologos D, Tsitoura I, Kouloumpis V, Tsoutsos T. 2014. Visual impact assessment method for wind parks: a case study in Crete, Land Use Pol. 39: 110-120. https://doi.org/10.1016/j.landusepol.2014.03.014

Kunz TH, Arnett EB, Erickson WP, Hoar AR, Johnson GD, Larkin RP, Strickland MD, Thresher RW, Tuttle MD. 2007. Ecological impacts of wind energy development on bats: questions, research needs, and hypotheses. Frontiers in Ecology and the Environment 5: 315–324. https://doi.org/10.1890/1540-9295(2007)5[315:EIOWED]2.0.CO;2

Landau AN, Fries P. 2012. Attention Samples Stimuli Rhythmically. Current Biology 22: 1000–1004. https://doi.org/10.1016/j.cub.2012.03.054

Leung DYC, Yang Y. 2012. Wind energy development and its environmental impact: review. Renewable and Sustainable Energy Reviews 16(1): 1031-1039. https://doi.org/10.1016/j.rser.2011.09.024

Liang J, Grimm B, Goelz S, Bille J. 1994. Objective measurement of wave aberrations of the human eye with the use of a Hartmann-Shack wave-front sensor. J. Opt. Soc. Am. A 11: 1949-1957.

Liang J, Williams DR 1997. Aberrations and retinal image quality of the normal human eye. J. Opt. Soc. Am. A 14(11): 2873-2883.

Lloret J, Wawrzynkowski P, Dominguez-Carrió C, Sardá R, Molins C, Gili JM, Sabatés A, Vila-Subirós J, Garcia L, Solé J, Berdalet E, Turiel A, Olivares A. 2023. Floating offshore wind farms in Mediterranean marine protected areas: a cautionary tale. ICES Journal of Marine Science, 2023: fsad131, https://doi.org/10.1093/icesjms/fsad131

Losada MA, Navarro R. 1998. Point spread function of the human eye obtained by a dual double-pass method. Pure Appl. Opt. 7: L7-L13.

Lothian A, 2008. Scenic perceptions of the visual effects of wind farms on South Australian landscapes, Geographical Research 46: 196-207. https://doi.org/10.1111/j.1745-5871.2008.00510.x

Marín C, Jafari J. 2008. *StarLight: A Common Heritage*. Canary Islands, Spain: StarLight Initiative La Palma Biosphere Reserve, Instituto De Astrofísica De Canarias, Government of The Canary Islands, Spanish Ministry of The Environment, UNESCO-MaB.

Marques AT, Batalha H, Rodrigues S, Costa H, Ramos-Pereira MJ, Fonseca C, Mascarenhas M, Bernardino J. 2014. Understanding bird collisions at wind farms: An updated review on the causes and possible mitigation strategies. Biological Conservation 179: 40–52. https://doi.org/10.1016/j.biocon.2014.08.017

Navarro R, Losada MA. 1997a. Aberrations and relative efficiency of light pencils in the living human eye. Optom. & Vis. Sci. 74: 540-547.

Navarro R, Losada MA. 1997b. Shape of stars and optical quality of the human eye. J. Opt. Soc. Am. A 14: 353-359.

Navarro R, Moreno E, Dorronsoro C. 1998. Monochromatic aberrations and point-spread functions of the human eye across the visual field. J. Opt. Soc. Am. A 15: 2522-2529.

NPS. 2021. Natural Sounds and Night Skies Division. US National Parks Service. https://www.nps.gov/orgs/1050/index.htm [Accessed 26 September 2023]

Pogson N. 1856. Magnitude of 36 of the minor planets. Monthly Notices of the Royal Astronomical Society 17(1): 12–15, https://doi.org/10.1093/mnras/17.1.12.

Pohl J, Hübner G, Mohs A. 2012. Acceptance and stress effects of aircraft obstruction markings of wind turbines. Energy Pol. 50: 592e600. https://doi.org/10.1016/j.enpol.2012.07.062

Pohl J, Rudolph D, Lyhne I, Clausen NE, Aaen SB, Hübner G, Kørnøv L, Kirkegaard JK. 2021. Annoyance of Residents Induced by Wind Turbine Obstruction Lights: A Cross-Country Comparison of Impact Factors. Energy Policy 156: 112437. https://doi.org/10.1016/j.enpol.2021.112437

Porter J, Guirao A, Cox IG, Williams DR. 2001. Monochromatic aberrations of the human eye in a large population. J. Opt. Soc. Am. A 18: 1793-1803.

Rich C, Longcore T (ed.). 2006. Ecological consequences of artificial night lighting. Washington, D.C.: Island Press. p. 1.

Rodrigues L, Bach L, Dubourg-Savage MJ, Karapandža B, Rnjak D, Kervyn T, Dekker J, Kepel A, Bach P, Collins J, Harbusch C, Park K, Micevski B, Minderman J. 2015. Guidelines for consideration of bats in wind farm projects – Revision 2014. EUROBATS Publication Series No. 6, Bonn, Germany: EUROBATS Secretariat. Available from: EUROBATS_6_wind turbines_engl_web_neu.pdf [Accessed 26 September 2023]

Rudolph D, Kirkegaard J, Lyhne I, Clausen NE, Kørnøv L. 2017. Spoiled darkness? Sense of place and annoyance over obstruction lights from the world's largest wind turbine test centre in Denmark. Energy Res. Social Sci. 25 :80e90. https://doi.org/10.1016/j.erss.2016.12.024

Saidur R, Rahim NA, Islam MR, Solangi KH. 2011. Environmental impact of wind energy. Renew. Sustain. Energy Rev. 15(5): 2423e2430. https://doi.org/10.1016/j.rser.2011.02.024

Schaefer BE. 1993. Astronomy and the Limits of Vision. Vistas in Astronomy 36: 311- 361. http://dx.doi.org/10.1016/0083-6656(93)90113-X

Smallwood KS. 2013. Comparing bird and bat fatality-rate estimates among North American wind-energy projects. Wildlife Society Bulletin 37: 19–33. https://doi.org/10.1002/wsb.260

Teillet PM. 1990. Rayleigh optical depth comparisons from various sources- Appl. Opt. 29: 1897-1900 https://doi.org/10.1364/AO.29.001897

Thibos LN, Hong X, Bradley A, Cheng X. 2002. Statistical variation of aberration structure and image quality in a normal population of healthy eyes. Journal of the Optical Society of America A, 19(12): 2329-2348.

Thibos LN, Bradley A, Hong X. 2002. A statistical model of the aberration structure of normal, well-corrected eyes. Ophthal. Physiol. Opt. 22: 427–433

van den Berg TJTP, Franssen L, Coppens JE. 2010. Ocular Media Clarity and Straylight. In Darlene A. Dartt (ed), *Encyclopedia of the Eye*, Vol 3. Oxford, UK: Academic Press. pp. 173-183.

van den Berg TJTP, Franssen L, Kruijt B, Coppens JE. 2013. History of ocular straylight measurement: A review. Zeitschrift für Medizinische Physik 23: 6–20. https://doi.org /10.1016/j.zemedi.2012.10.009

Voigt CC, Kaiser K, Look S, Scharnweber K, Scholz C. 2022. Wind turbines without curtailment produce large numbers of bat fatalities throughout their lifetime: A call against ignorance and neglect. Global Ecology and Conservation 37: e02149. https://doi.org/10.1016/j.gecco.2022.e02149